An experimental study of the effect of water and chlorine on plagioclase nucleation and growth in mafic magmas: application to mafic pegmatites

Paul Heckmann, Giada Iacono-Marziano, Sabina Strmić Palinkaš

Eur. J. Mineral., 35, 1111–1124, 2023
https://doi.org/10.5194/ejm-35-1111-2023

European Journal of Mineralogy
Open Access

Research article

An experimental study of the effect of water and chlorine on plagioclase nucleation and growth in mafic magmas: application to mafic pegmatites

Paul Heckmann[1], **Giada Iacono-Marziano**[1,2], **and Sabina Strmić Palinkaš**[1,3]

[1]Department of Geosciences, UiT The Arctic University of Norway, Dramsvegen 201, 9037 Tromsø, Norway
[2]ISTO, UMR 7327 CNRS-Université d'Orléans-BRGM, 1A rue de la Ferollerie,
45071 Orléans CEDEX 2, France
[3]Department of Earth Science, University of Bergen, Allégaten 41, 5007 Bergen, Norway

Correspondence: Paul Heckmann (paul.heckmann@uit.no)

Received: 26 May 2023 – Revised: 6 October 2023 – Accepted: 17 October 2023 – Published: 13 December 2023

Abstract. In this study, the effects of H_2O and Cl on the grain size and nucleation delay of plagioclase in basaltic magma were investigated using dynamic and equilibrium experiments at 1150 °C, 300 MPa, and oxygen fugacity between FMQ − 1.65 and FMQ + 0.05 (fayalite–magnetite–quartz). Each experiment consisted of five samples of basaltic composition (from the Hamn intrusion in Northern Norway) containing varying amounts of H_2O (up to 2 wt %) and Cl (up to 1 wt %). The equilibrium experiments were used as a reference frame for the phase assemblage, geochemical composition, and liquidus temperatures and were compared to thermodynamic models using MELTS software. Experimental phase abundances and plagioclase compositions are in good agreement with the predictions of MELTS. The dynamic experiments were initially heated above the liquidus temperature to destroy crystal nuclei and then kept at 1150 °C for 100, 250, or 1800 min. These experiments show that as the concentration of H_2O in the melt increases, plagioclase nucleation is delayed, plagioclase abundance decreases, but its size increases. Therefore, the addition of H_2O seems to favor plagioclase growth at the expense of nucleation. Thermodynamic and kinetic calculations corroborate an increase in the nucleation delay of plagioclase with increasing H_2O content dissolved in the melt, suggesting that H_2O decreases the undercooling of the silicate melt. The addition of Cl also seems to delay plagioclase nucleation, although this is not supported by kinetic calculations. Increasing the Cl content decreases plagioclase abundance but does not significantly affect its size.

The homogeneous pegmatitic pockets of the mafic–ultramafic Hamn intrusion exhibit several petrological and geochemical features, suggesting that H_2O and Cl enrichment in the silicate melt was the origin of the pegmatitic texture. The experimental results presented here indicate that H_2O, rather than Cl, may have played an important role in the formation of the pegmatitic texture.

1 Introduction

Pegmatites are igneous rocks with extremely large grains and/or highly directional growth habits (London, 2008). Pegmatites are most commonly felsic in composition, although mafic pegmatites have also been reported and can be found as either unzoned pocket clusters that differ only in grain size from their host rock or in their texturally and mineralogically zoned bodies (Beard, 1986; Beard and Scott, 2018; Larsen and Brooks, 1994; Pentek et al., 2006). The Paleoproterozoic mafic–ultramafic Hamn intrusion in Senja (Northern Norway) contains zoned and unzoned pegmatites (Heckmann et al., 2022). The zoned pegmatites exhibit mineralogical and textural zonation, as well as evidence of undercooling of the pegmatite-forming magma, whereas the unzoned pegmatites do not. The major and trace element compositions, rock-forming mineral assemblages, and mineral chemistries of the unzoned pegmatitic pockets (less than 1 m in diameter) are similar to those of their host gabbronorite. Unzoned pegmatites, however, can be distinguished from their host rock

by abundant epidotization and scapolitization, implying that H_2O- and Cl-bearing fluids were required for the formation of the pegmatitic texture (Heckmann et al., 2022).

This is consistent with the prevailing hypothesis proposed for the formation of pegmatitic textures that suggests an important role of volatiles in pegmatite-forming processes (Bartels et al., 2015, 2013, 2011; Jahns and Burnham, 1969; London, 1984; Thomas et al., 2003; Nabelek et al., 2010). Fluxing components, such as H_2O, can lower crystallization temperatures, nucleation rates, melt polymerization, and melt viscosity while increasing diffusion rates (Fenn, 1977; Mysen and Richet, 2005; Shaw, 1963; Watson and Baker, 1991), and they may thus be the critical factor causing coarse grain size or directional growth habits. In particular, most studies on the petrogenesis of mafic pegmatites from various locations concluded that pegmatites formed by a locally segregated hydrous melt (Pentek et al., 2006) or intercumulus melt in the presence of a fluid phase (Beard, 1986; Larsen and Brooks, 1994). For example, the gabbroic pegmatite of the Smartville Complex in California shows epidotization of plagioclase, similar to the unzoned pegmatite of Hamn (Beard, 1986). Furthermore, elevated Cl concentrations associated with mafic pegmatites have been reported in a variety of contexts (Meurer and Boudreau, 1996; Pentek et al., 2006; Sonnenthal, 1992). The presence of a Cl-bearing fluid phase in the Hamn pegmatite and other mafic pegmatites around the world begs the question of how H_2O and Cl affect the growth and thus the texture of rock-forming minerals. We present an experimental study that investigated the effect of H_2O and Cl dissolved in silicate melts on crystal grain size, nucleation delay, and crystallization order in gabbronoritic melts. We used a natural composition from the Hamn intrusion in Northern Norway to determine whether H_2O and Cl enrichment in the silicate melt caused the formation of unzoned pegmatites at Hamn, as suggested by mineralogical and geochemical data.

2 Methods

2.1 Starting material

The starting material was the gabbronorite host rock of the homogeneous pegmatites of the mafic–ultramafic Hamn intrusion in Senja, Northern Norway (sample KR-HM-28 from Heckmann et al., 2022), which was melted for 2 h at 1 atm and 1600 °C before being quenched to a crystal and bubble-free glass. Table 1 shows the bulk major element analysis of gabbronorite (Heckmann et al., 2022) and the electron microprobe analysis of the starting glass.

2.2 Experimental strategy

Five experimental runs were carried out at 300 ± 10 MPa with varying time–temperature paths (Table 2). In the "equilibrium experiments", the samples were heated directly to the target temperature of 1150 °C, followed by an 1800 min dwell ramp and a rapid quench. In the "dynamic experiments", the samples were heated above the liquidus temperature (1275 °C) for 10 min and then cooled to the target temperature of 1150 °C (at a rate of 10 °C min^{-1}). The samples were held at 1150 °C for three different durations (100, 250, and 1800 min) before being rapidly quenched. An additional nominally anhydrous sample was heated to 1275 °C for 10 min before rapid quenching. The pressure of 300 MPa was chosen to be relevant to the emplacement of mafic pegmatites, estimated to be between 100 and 500 MPa for the Smartville Complex (Beard, 1986) and 600 MPa for the Hamn intrusion (Heckmann et al., 2022). Each experimental run included five samples spiked with varying amounts of deionized H_2O and AgCl (the latter served as a source of chlorine). The starting glass powder was loaded into Pt or $Au_{80}Pd_{20}$ capsules (internal diameter 2.5 or 2.7 mm), together with variable H_2O and Cl contents (up to 2.1 wt % H_2O and 1.0 wt % Cl; Table 2). To be relevant to natural magmas, the Cl-bearing samples also contained 1.0 wt % H_2O. A total of 1 wt % chlorine was chosen because it is close to but slightly below the upper limit of around 2 wt % for chlorine contents in basaltic melts (Webster et al., 2018).

The "equilibrium experiments" were typical phase equilibrium experiments used to characterize the mineral phases that occur at 1150 °C, as well as their abundances. The "dynamic experiments" were heated above the liquidus temperature to destroy all crystal nuclei before cooling to the target temperature to show the effect of H_2O and Cl on the nucleation delay of the mineral phases. A temperature of 1150 °C was chosen to observe the onset of plagioclase and pyroxene crystallization. The additional experiment at 1275 °C showed the absence of crystals, confirming that the anhydrous liquidus of the selected composition is lower than 1275 °C.

Table 1. Major oxide composition of starting material.

	PH-HM-28*	Starting glass**
SiO_2	52.19	51.5 (9)
TiO_2	0.48	0.54 (6)
Al_2O_3	20.05	20.0 (6)
FeO_{tot}	6.05	6.2 (3)
	5.50	5.9 (1)
CaO	10.69	11.0 (1)
Na_2O	3.45	3.5 (1)
K_2O	0.35	0.38 (3)
P_2O_5	0.03	n.d.
LOI	0.59	n.d.
Total	99.38	99.1 (4)

* Host rock gabbronorite (Heckmann et al., 2022).
** Analyzed by electron microprobe (EMP), 18 analyses. The abbreviation n.d. signifies not determined. Numbers in brackets are the standard deviation on the last decimal unit. LOI signifies loss of ignition.

Table 2. Experimental conditions and phase proportions.

Sample	Capsule	Exp. type	Duration (min)	H_2O loaded (wt %)[a]	Cl loaded (wt %)[a]	fO_2 (ΔFMQ)[b]	fO_2 (ΔFMQ)[b]	Phases (wt %)[c]	Calc. Fe loss (wt %)[d]
PEG_46	AuPd	Equilibrium	1800	0	0	n.d.	n.d.	glass (68), pl (27), cpx (4), ol (1)	31
PEG_36	AuPd	Dynamic	100	0	0	n.d.	n.d.	glass (82), pl (18)	21
PEG_21	Pt	Dynamic	250	0	0	n.d.	n.d.	glass (57), pl (36), cpx (6), ol (1)	15
PEG_41	AuPd	Dynamic	1800	0	0	n.d.	n.d.	glass (81), pl (19)	33
PEG_52	AuPd	Equilibrium	1800	1.0	0	-1.65 ± 0.25	-1.7 ± 0.3	glass (95), pl (5)	20
PEG_37	AuPd	Dynamic	100	1.0	0	-0.84 ± 0.20	-0.8 ± 0.2	glass (95), pl (5)	15
PEG_22	Pt	Dynamic	250	1.0	0	-1.15 ± 0.25	-1.2 ± 0.3	glass (90), pl (10)	22
PEG_42	AuPd	Dynamic	1800	1.0	0	-1.05 ± 0.20	-1.1 ± 0.2	glass (98), pl (2)	22
PEG_48	AuPd	Equilibrium	1800	2.0	0	-0.8 ± 0.1	-0.8 ± 0.1	glass (96), pl (4)	18
PEG_40	AuPd	Dynamic	100	2.0	0	0.05 ± 0.10	0.1 ± 0.1	glass (100)	9
PEG_25	Pt	Dynamic	250	1.9	0	-0.1 ± 0.1	-0.1 ± 0.1	glass (100)	22
PEG_45	AuPd	Dynamic	1800	2.0	0	-0.17 ± 0.10	-0.2 ± 0.1	glass (100)	18
PEG_55	AuPd	Equilibrium	1800	1.0	0.4	-1.65 ± 0.25	-1.7 ± 0.3	glass (95), pl (5)	34
PEG_39	AuPd	Dynamic	100	1.0	0.4	-0.84 ± 0.20	-0.8 ± 0.2	glass (100), pl (traces)	12
PEG_24	Pt	Dynamic	250	1.0	0.4	-0.95 ± 0.15	-1.0 ± 0.2	glass (95), pl (5)	31
PEG_44	AuPd	Dynamic	1800	1.0	0.4	-1.05 ± 0.20	-1.1 ± 0.2	glass (98), pl (2)	24
PEG_54	AuPd	Equilibrium	1800	0.8	1.0	-1.65 ± 0.25	-1.7 ± 0.3	glass (97), pl (3)	19
PEG_38	AuPd	Dynamic	100	1.0	1.0	-0.84 ± 0.20	-0.8 ± 0.2	glass (100)	12
PEG_23	Pt	Dynamic	250	1.0	1.0	-0.95 ± 0.15	-1.0 ± 0.2	glass (100), pl (traces)	32
PEG_43	AuPd	Dynamic	1800	0.9	1.0	-1.05 ± 0.20	-1.1 ± 0.2	glass (100), pl (traces)	22

All samples were run at 1150 °C and 300 MPa (temperature and pressure uncertainties were ± 5 °C and ± 10 MPa, respectively). [a] Amounts of water and chlorine loaded in the capsule. [b] Oxygen fugacity calculated from solid sensor composition and melt H_2O content. [c] Phase proportions determined by mass balance. [d] Fe loss is the percentage of the difference between the FeO content of the normalized starting glass and the estimated starting glass that has been calculated by means of mass balance. The abbreviation n.d. signifies not determined.

Experiments were carried out at the Institut des Sciences de la Terre d'Orléans (ISTO) in internally heated pressure vessels equipped with rapid quenching devices. The vessels were pressurized with H_2–Ar mixtures, and the oxygen fugacity (fO_2) was varied by varying the H_2 partial pressure in the vessel and monitored using the Co–Pd–O solid sensor technique (Taylor et al., 1992). Two pellets of CoPd metal mixtures (each with a different Co / Pd ratio) and CoO were placed in a Pt capsule filled with Zr oxide in the presence of excess H_2O and run under the same conditions as the samples. The fO_2 of the sensor was calculated from the composition of its metallic phases (only Pt-free analyses were considered), as described by Pownceby and O'Neill (1994). The fO_2 of each charge was calculated from the activity of H_2O estimated for each charge, as described by Botcharnikov et al. (2008), using the model of Iacono-Marziano et al. (2012). Table 2 shows the oxygen fugacity values in logarithmic units relative to the fayalite–magnetite–quartz (FMQ) buffer.

2.3 Analytical techniques

The mineral phases and textural features of the recovered and polished samples were studied using a Zeiss Merlin Compact field emission gun scanning electron microscope (FEG-SEM) at the ISTO. The major element compositions of the minerals, glasses, and redox sensors were analyzed using a Cameca SX Five electron microprobe at the ISTO. The following operating conditions were used for the glasses and silicate minerals: 15 kV accelerating voltage, 10 nA beam current, 10 s counting time for all elements, 6–12 m spot size for glasses, and a focused beam for minerals. To limit losses, sodium and potassium levels were first analyzed. The redox sensor alloys were analyzed at 15 kV, 20 nA, 10 s counting for all elements, and a focused beam. Table S1 lists the standards and detection limits that were used. The software Fiji was used to perform textural analyses of the run products on backscattered electron (BSE) images (Schindelin et al., 2012).

2.4 Thermodynamic and kinetic calculations

Thermodynamic modeling was performed to simulate crystallization at 300 MPa and FMQ -1 ± 1 for 0 wt %, 025 wt %, 1 wt %, and 2 wt % H_2O, using the software rhyolite-MELTS v.1.2.0 (Ghiorso and Sack, 1995; Gualda et al., 2012; Ghiorso and Gualda, 2015). Although the incorporation of Cl in MELTS is purely exploratory, as stated in the software manual, additional simulations were conducted for H_2O contents of 1 wt % and Cl contents of 0.4 wt % and 1 wt %.

The simulations show that 1150 °C is below the liquidus temperature for each H_2O and Cl combination used in our experiments (Table S2). The results of the simulations were compared with the results of the "equilibrium experiments" in terms of phase abundance and composition and served as input parameters (Gibbs free energy (ΔG) of formation and viscosity of the melt) for the nucleation delay calculation (see below).

In natural magmas, crystal nucleation is likely delayed until the new phase becomes thermodynamically stable. We calculated the plagioclase and clinopyroxene nucleation delays

(τ) using the model of Rusiecka et al. (2020):

$$\tau = \frac{16\,\mathrm{h}}{\pi} \frac{\sigma}{\Delta G_{\mathrm{V}}^2 a^4} \cdot \exp\left(\frac{\Delta G_{\mathrm{D}}}{k_{\mathrm{b}} T}\right), \quad (1)$$

where h is Planck's constant, σ is the interfacial free energy per unit area, ΔG_{V}^2 is the bulk free energy per unit volume, ΔG_{D} is Gibbs free energy of the formation of the mineral, a is the size of a structural unit, k_{b} is Boltzmann's constant, and T is temperature. ΔG_{D} can be substituted for the activation energy (E_{A}), using the Eyring or Stokes–Einstein equation:

$$E_{\mathrm{A}} = -k_{\mathrm{b}} T \ln\left(\frac{h}{\mathrm{a}^3 \eta}\right), \quad (2)$$

where η is viscosity.

We used an interface free energy of $0.18\,\mathrm{J\,m^{-2}}$ for plagioclase (Nabelek et al., 1978) and $0.33\,\mathrm{J\,m^{-2}}$ for clinopyroxene (Baker et al., 2020). The size of structural unit a was set to the Si^{4+} ionic radius of 0.26×10^{-10} m (Shannon, 1976). ΔG_{V} was calculated from a molar volume of $1.01 \times 10^{-4}\,\mathrm{m^3\,mol^{-1}}$ for plagioclase (arithmetic mean of value for albite and anorthite) and of $6.61 \times 10^{-5}\,\mathrm{m^3\,mol^{-1}}$ for diopside (Robie and Bethke, 1962). The Gibbs free energy (ΔG) of formation and the viscosity were calculated using MELTS software. The heterogeneous nucleation delay (τ_{het}) was also calculated from the homogeneous nucleation delay (τ), considering that minerals can nucleate on pre-existing mineral phases or the noble metal capsule wall (Fokin et al., 2006). For example, clinopyroxene is likely to nucleate on pre-existing plagioclase surfaces:

$$\tau_{\mathrm{het}} = \tau \varphi^{1/3}, \quad (3)$$

where

$$\varphi = \frac{1}{2} - \frac{3}{4}\cos\theta + \frac{1}{4}\cos^3\theta \quad (4)$$

and θ is the interior contact angle between the surface upon which nucleation occurs and the nucleating phase. Θ was set to 45°, based on an optical estimate of the average contact angle to calculate the average delay for heterogeneous nucleation.

Two assumptions were necessary to simplify these calculations: (i) volume and surface thermodynamic properties of the nuclei of the new phase are considered size-independent and equal to the respective values of the corresponding macroscopic crystals, although experimental results often show discrepancies (Fokin et al., 2010; Rusiecka et al., 2020); and (ii) the interface between the growing nucleus and parent phase is considered a sharp boundary, although it may have a diffuse or curved nature.

3 Results

At the end of each experiment, all recovered capsules were weighed to check for possible leaks, pierced, and re-weighed to check for the presence of a fluid phase. The lack of weight loss after piercing and heating at 120 °C indicated that no fluid phase was present, implying that the loaded volatiles were completely dissolved in the silicate melt. Table 2 shows the phase proportions calculated by mass balance from the phase compositions, whereas Tables 3 and 4 show the phase compositions analyzed by electron microprobe. The H_2O content of the silicate glasses was also estimated using mass balance based on the initial amount of H_2O loaded into the capsule and the crystal content. Submicron-sized blebs of Ag are visible in samples spiked with 1 wt % Cl ($\sim$ 4 wt % AgCl), both in the silicate glass and as inclusions in plagioclase crystals. The Fe loss from the melt to the capsule material was calculated by mass balance (Table 2). It does not show simple relationships with time and capsule material and is therefore unpredictable (Fig. S1 in the Supplement). The effect of Fe loss was investigated by performing MELTS simulations with a reduced Fe content (Table S3). Although Fe losses exceeding 30 wt % are estimated for five samples, variations in phase equilibria for the reduced Fe-content calculated with MELTS are extremely low (Table S3).

3.1 Equilibrium experiments

The compositions of the phases (crystals and glasses) within a given sample display considerable chemical uniformity, except for Cl, which shows a heterogeneous distribution and enrichment towards the lower part of the capsule, where AgCl is likely to be concentrated. Consequently, it is highly probable that the 1800 min experiments approached a state of partial equilibrium, consistent with previous research on phase equilibria in hydrous basalts conducted at similar temperatures. These earlier investigations employed shorter experimental durations, typically less than 24 h, as exemplified by the studies of Sisson and Grove (1993) and Di Carlo et al. (2006).

The plagioclase crystals of the samples from the equilibrium experiment are 4–7 µm in length, with a mean length-to-width ratio of 2–4 (Fig. 1a–c). Crystallization of silicate phases decreased with increasing H_2O content (Fig. 1a–c; Table 2). H_2O addition reduced plagioclase crystallization (Fig. 3a) and suppressed olivine and clinopyroxene crystallization (Fig. 1a–c; Table 2). On the other hand, Cl does not appear to affect the degree of crystallization or phase stability (Figs. 2a–c and 4; Table 2). The anorthite content of plagioclase increased with H_2O addition as the plagioclase content decreased (Fig. 3b).

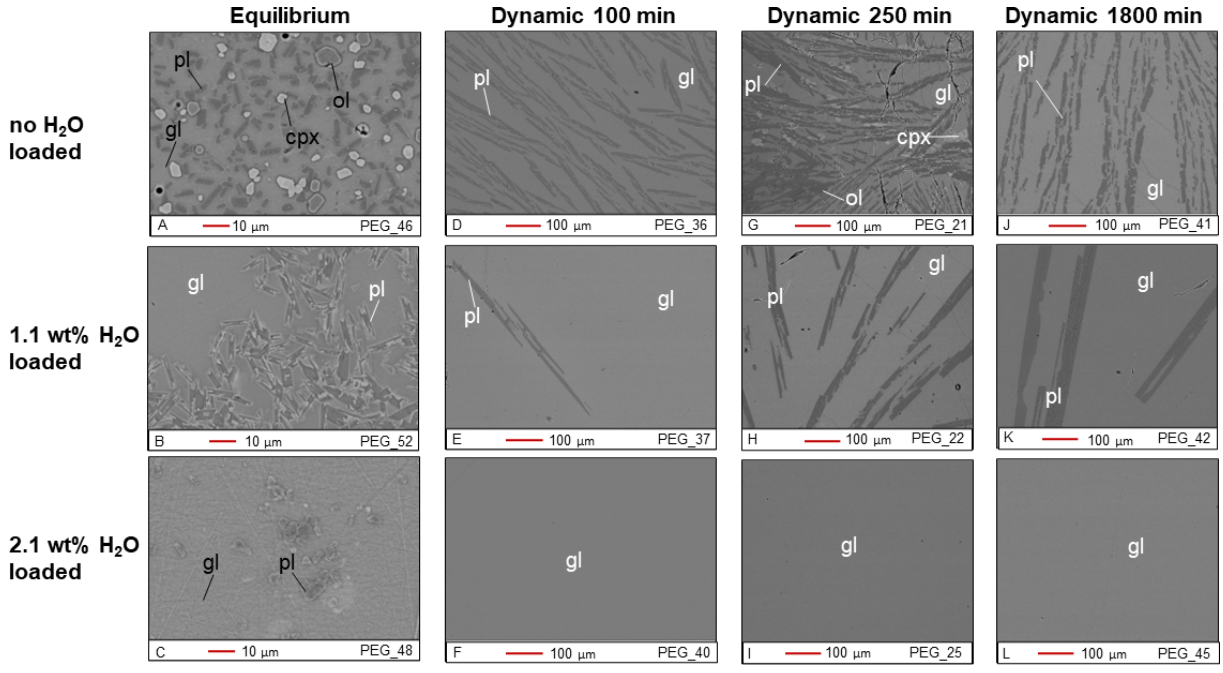

Figure 1. BSE images of Cl-free samples from the equilibrium experiment **(a–c)** and the dynamic experiments **(d–l)**. gl: glass; pl: plagioclase; cpx: clinopyroxene; ol: olivine.

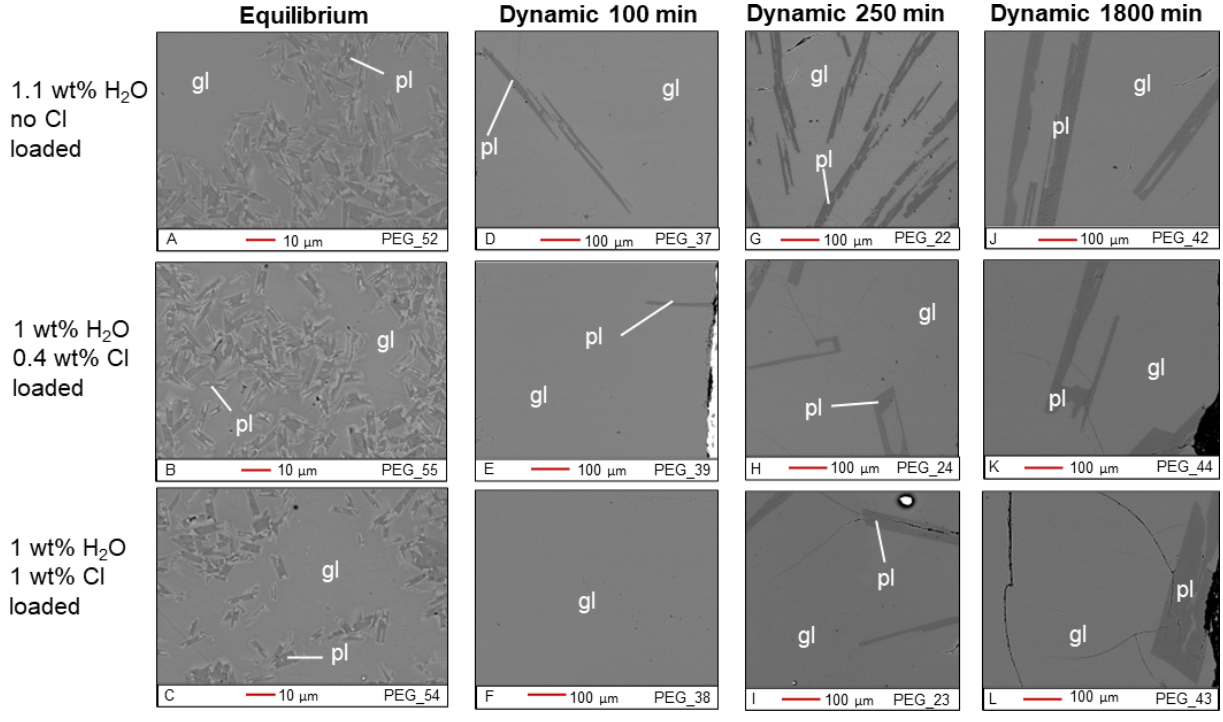

Figure 2. BSE images of Cl-bearing samples from the equilibrium experiment **(a–c)** and the dynamic experiments **(d–l)**. gl: glass; pl: plagioclase.

Table 3. Experimental samples without Cl.

Sample		n	SiO_2^*	TiO_2^*	$Al_2O_3^*$	FeO_{tot}^*	MgO*	CaO*	Na_2O*	K_2O*	Tot*	H_2O**	An
PEG_46	Glass	21	53.5 (6)	0.60 (7)	17.7 (5)	5.3 (3)	6.0 (2)	9.4 (3)	3.8 (1)	0.51 (4)	97.0 (6)	–	
	Pl	11	51.6 (3)	–	29.0 (4)	0.7 (1)	0.7 (2)	13.4 (4)	3.9 (2)	0.10 (4)	99.4 (4)		0.65 (2)
	Cpx	13	50.9 (9)	0.7 (2)	5.4 (9)	8.2 (4)	17 (1)	17.5 (8)	0.6 (1)	–	100.6 (8)		
	Olivine	15	40.3 (5)	–	–	11.3 (5)	48.1 (5)	0.4 (1)	–	–	100.6 (6)		
PEG_36	Glass	30	52.2 (4)	0.6 (1)	18 (1)	5.9 (5)	7.1 (7)	10.2 (3)	3.37 (9)	0.46 (7)	97.7 (7)	–	
	Pl	24	51.3 (5)	–	30.1 (4)	0.6 (2)	0.4 (1)	13.5 (2)	3.7 (1)	0.07 (3)	99.6 (6)		0.67 (1)
PEG_21	Glass	11	51.5 (6)	0.69 (8)	16.6 (2)	7.3 (5)	6.9 (2)	8.9 (1)	3.6 (1)	0.58 (4)	96.1 (6)	–	
	Pl	12	51.8 (4)	–	28.1 (4)	1.7 (2)	0.31 (3)	12.8 (3)	3.9 (2)	0.10 (2)	98.7 (4)		0.64 (1)
	Cpx	14	49 (1)	0.5 (1)	5.4 (6)	7 (1)	18 (1)	18 (2)	0.41 (5)	–	99.2 (5)		
	Olivine	5	40.1 (5)	–	–	9.7 (4)	50.3 (4)	0.3 (1)	–	–	100.8 (6)		
PEG_41	Glass	40	52.8 (4)	0.64 (7)	17.7 (2)	5.1 (4)	7.3 (1)	10.1 (1)	3.55 (8)	0.44 (6)	97.7 (5)	–	
	Pl	24	51.4 (7)	–	29.8 (7)	0.4 (2)	0.4 (2)	13.7 (4)	3.7 (2)	0.09 (4)	99.6 (7)		0.67 (2)
PEG_52	Glass	10	52.0 (4)	0.5 (1)	19.2 (1)	5.2 (2)	5.9 (1)	10.4 (1)	3.5 (1)	0.41 (5)	97.2 (3)	1.03	
	Pl	8	49.9 (9)	–	31.0 (7)	0.6 (1)	0.5 (1)	15.1 (7)	2.9 (4)	0.06 (3)	100.1 (3)		0.74 (2)
PEG_37	Glass	29	51.1 (4)	0.47 (7)	19.8 (2)	5.5 (2)	5.74 (5)	10.6 (1)	3.35 (8)	0.36 (6)	97.2 (4)	1.02	
	Pl	18	50.0 (4)	–	31.0 (3)	0.47 (9)	0.23 (3)	14.4 (2)	3.2 (1)	0.05 (4)	99.3 (6)		0.71 (2)
PEG_22	Glass	13	51.7 (5)	0.51 (4)	18.5 (5)	5.3 (4)	6.1 (2)	10.1 (2)	3.43 (9)	0.44 (3)	96.3 (4)	1.00	
	Pl	31	49.6 (8)	–	30.8 (9)	0.5 (2)	0.25 (7)	14.5 (3)	3.1 (2)	0.04 (3)	99 (1)		0.72 (1)
PEG_42	Glass	28	51.6 (3)	0.50 (8)	19.4 (5)	5.0 (3)	6.0 (2)	10.52 (9)	3.51 (9)	0.36 (4)	97.0 (4)	0.99	
	Pl	35	49.6 (5)	–	31.5 (4)	0.29 (8)	0.20 (2)	14.8 (4)	3.1 (2)	0.06 (2)	99.6 (6)		0.73 (2)
PEG_48	Glass	10	50.6 (3)	0.42 (5)	19.5 (7)	5.0 (3)	5.7 (3)	10.6 (4)	3.5 (1)	0.34 (5)	95.7 (4)	2.00	
	Pl	8	47.6 (9)	–	32.3 (9)	0.7 (2)	0.5 (3)	16.5 (7)	2.1 (4)	0.05 (4)	99.9 (4)		0.81 (3)
PEG_40	Glass	25	50.4 (4)	0.47 (6)	19.6 (1)	5.6 (2)	5.69 (7)	10.5 (1)	3.34 (8)	0.38 (4)	96.1 (5)	1.91	
PEG_25	Glass	14	50.9 (2)	0.47 (4)	19.4 (3)	4.8 (3)	5.60 (6)	10.6 (1)	3.25 (7)	0.36 (2)	95.5 (3)	1.85	
PEG_45	Glass	24	50.9 (4)	0.46 (7)	19.7 (2)	5.0 (3)	5.57 (8)	10.54 (9)	3.44 (6)	0.35 (4)	96.2 (4)	1.88	

The abbreviation n signifies number of analyses. Numbers in brackets are the standard deviation on the last decimal unit. * Average compositions of the different phases occurring in the experimental samples analyzed by EMP (wt %). ** Water content of the melt estimated by mass balance. An signifies anorthite content of plagioclase.

Table 4. Experimental samples with Cl.

Sample		n	SiO_2^*	TiO_2^*	$Al_2O_3^*$	FeO*	MgO*	CaO*	Na_2O*	K_2O*	Cl*	Tot*	H_2O**	An
PEG_54	Glass	10	51.5 (2)	0.49 (5)	19.5 (3)	5.1 (2)	5.72 (6)	10.4 (2)	3.46 (6)	0.38 (5)	1.09 (5)	97.7 (4)	0.80	
	Pl	9	49.2 (9)	–	31.0 (7)	0.6 (1)	0.5 (2)	15.4 (6)	2.6 (3)	0.06 (3)	–	99.6 (4)		0.76 (2)
PEG_39	Glass	25	51.1 (4)	0.48 (6)	19.8 (2)	5.4 (2)	5.76 (9)	10.6 (1)	3.27 (7)	0.36 (5)	0.5 (5)	97.0 (7)	0.97	
	Pl	4	49.5 (4)	–	31.8 (4)	0.5 (2)	0.24 (7)	15.0 (4)	2.94 (9)	0.02 (2)	–	100.0 (2)		0.74 (1)
PEG_24	Glass	13	51.9 (5)	0.49 (4)	19.2 (4)	4.5 (4)	5.8 (2)	10.2 (1)	3.40 (8)	0.41 (4)	0.7 (1)	96.7 (4)	1.01	
	Pl	13	49.8 (5)	–	30.9 (3)	0.5 (2)	0.22 (2)	14.4 (4)	3.1 (2)	–	–	99.1 (3)		0.72 (2)
PEG_44	Glass	26	51.2 (7)	0.49 (9)	19.5 (5)	4.7 (3)	5.7 (2)	10.6 (2)	3.5 (2)	0.36 (4)	0.5 (7)	96.7 (4)	0.94	
	Pl	34	49.5 (3)	–	31.8 (4)	0.3 (1)	0.19 (2)	15.1 (2)	3.0 (1)	0.04 (3)	–	99.9 (4)		0.74 (1)
PEG_55	Glass	10	52.3 (3)	0.49 (3)	18.5 (3)	4.3 (3)	5.9 (2)	9.9 (2)	3.25 (8)	0.42 (3)	1.1 (2)	96.3 (6)	1.07	
	Pl	10	50 (1)	–	30 (1)	0.7 (3)	0.44 (2)	15 (1)	3.0 (6)	0.06 (1)	–	99.0 (2)		0.73 (3)
PEG_38	Glass	25	50.4 (6)	0.45 (8)	19.6 (2)	5.4 (3)	5.67 (9)	10.4 (1)	3.33 (9)	0.37 (4)	1.2 (5)	97.1 (5)	0.96	
PEG_23	Glass	15	51.0 (7)	0.46 (3)	19.5 (3)	4.1 (3)	5.50 (9)	10.4 (1)	3.23 (8)	0.35 (2)	1.16 (9)	96 (1)	0.95	
	Pl	14	49.1 (4)	–	31.4 (5)	0.25 (8)	0.20 (2)	15.0 (2)	2.8 (1)	0.04 (2)	–	99.0 (8)		0.74 (1)
PEG_43	Glass	25	50.9 (8)	0.47 (9)	19.7 (4)	4.8 (3)	5.7 (2)	10.5 (1)	3.5 (2)	0.36 (4)	1.0 (9)	97.1 (5)	0.91	
	Pl	14	49.5 (4)	–	31.9 (2)	0.29 (8)	0.20 (2)	15.3 (2)	2.82 (9)	0.04 (2)	–	100.1 (4)		0.75 (2)

The abbreviation n signifies number of analyses. Numbers in brackets are the standard deviation on the last decimal unit. * Average compositions of the different phases occurring in the experimental samples analyzed by EMP (wt %). ** Water content of the melt estimated by mass balance. An signifies anorthite content of plagioclase.

3.2 Dynamic experiments

Crystallization was reduced in the dynamic experiments (Table 2; Figs. 1 and 2), and samples containing ~ 2 wt % H_2O are always crystal-free (Fig. 1f, i, l). The crystal sizes of the samples from the dynamic experiments are significantly larger than those from the equilibrium experiment: hundreds of microns ($\sim$ 150–300 µm) (Figs. 1 and 2). Plagioclase crystal shape also varies considerably from that of equilibrium samples: length-to-width ratios range from 8 to 23, with more skeletal forms in H_2O–(Cl-)-bearing samples (Figs. 1 and 2). Similar to the equilibrium experiment, H_2O reduced the amount of plagioclase crystallization (Fig. 3a). H_2O addition also increased plagioclase size; this is particularly clear in the samples that were held at 1150 °C for 1800 min (Fig. 4a, b): plagioclase length ranges from < 160 µm in the nominally anhydrous sample (Fig. 1j) up to > 300 µm in the samples with ~ 1 wt % dissolved H_2O (Fig. 1k). Olivine and clinopyroxene only occur in the sample with no added H_2O that was held at 1150 °C for 250 min (Fig. 1g) The nominally anhydrous sample that was held at 1150 °C for 100 min did not crystallize olivine and clinopyroxene, possibly owing to nucleation delay. In the dynamic experiments, Cl reduced the amount of plagioclase crystallization (Table 2; Figs. 2 and 3a); however, this did not seem to affect its size (Fig. 4b, c). Similar to the equilibrium experiments, the anorthite content of plagioclase increased with H_2O addition as the plagioclase content decreased (Fig. 3b). The Cl addition also appears to have increased the anorthite content, although variations are relatively limited (Fig. 3b).

3.3 MELTS modeling

The results of MELTS simulations at 1150 °C, 300 MPa, and FMQ are presented in Table 5 and Figs. 3 and 5 in terms of phase abundance and composition. Under these conditions, MELTS simulations predicted the crystallization of (i) clinopyroxene with two different compositions and plagioclase for 0 wt % H_2O and 0.25 wt % H_2O, (ii) clinopyroxene with only one composition and plagioclase for 1 wt % H_2O, and (iii) only plagioclase for 2 wt % H_2O (Table 5). The addition of Cl resulted in the suppression of clinopyroxene crystallization (Table 5). Simulations performed at the same temperature and pressure but with a lower oxygen fugacity (FMQ $-$ 2) show similar results for 0 wt % H_2O and 0.25 wt % H_2O (similar mineral abundances and chemistry; Supplement) but no clinopyroxene crystallization for 1 wt % H_2O and no plagioclase crystallization for 2 wt % H_2O. The suppression of clinopyroxene crystallization is possibly explained by decreases in the Fe^{3+} / Fe^{2+} ratio.

3.4 Nucleation delay calculations

The nucleation delays of plagioclase and clinopyroxene were calculated using the model of Rusiecka et al. (2020), in which the delay is determined by the barrier for the transition of a structural unit from the melt into the growing crystal nucleus. This barrier is represented by the activation energy of the diffusion of the nucleating crystal components in the silicate melt (see Sect. 2.4). We calculated nucleation delays for both homogeneous and heterogeneous nucleation. Homogeneous nucleation is a stochastic process that occurs with the same probability in any given volume element, whereas heterogeneous nucleation describes nucleation on preferred nucleation sites, such as pre-existing interfaces or surface defects (Fokin et al., 2006). Heterogeneous nucleation shortens the nucleation delay; therefore, the calculations (Table 6) include a correction coefficient that considers the interior contact angle between the nucleating surface and the nucleating material (Fokin et al., 2006). Our dynamic samples appear to have experienced heterogeneous nucleation at the capsule wall (e.g., Fig. 4b, c), but this does not rule out the possibility of homogeneous nucleation (e.g., Fig. 4a).

The calculated plagioclase nucleation delays are a few minutes under anhydrous conditions, a few tens of minutes when 1 wt % H_2O is present, and several hours when 2 wt % H_2O is present (Table 6). Clinopyroxene exhibits a nucleation delay of approximately 0.5–1 h under anhydrous conditions. Given that crystal nucleation is difficult to determine in dynamic experiments because of the extremely low number of crystals (e.g., Fig. 4b, c), this is in relatively good agreement with the delay estimated from our experimental results (Table 6).

4 Discussion

4.1 Equilibrium experiment versus MELTS predictions

The phase abundances and compositions of the equilibrium experiment were directly compared with those predicted using MELTS. We performed MELTS simulations with 0 and 0.25 wt % H_2O because nominally anhydrous samples synthesized in internally heated pressure vessels always contain a few 10ths of weight percentage of H_2O due to hydrogen diffusion through the Pt or AuPd capsules (Chou, 1986; Almeev et al., 2007). The results of the MELTS simulation using 0.25 wt % H_2O do, in fact, agree better with the nominally anhydrous sample's phase abundances and compositions. For this sample, the larger discrepancy with MELTS simulations is the occurrence of olivine crystallization, whereas MELTS predicted the crystallization of a second clinopyroxene for both 0 wt % H_2O and 0.25 wt % H_2O (Table 5). The co-crystallization of the two clinopyroxenes might be related to some general limitations of the MELTS algorithm. Moreover, plagioclase and clinopyroxene abun-

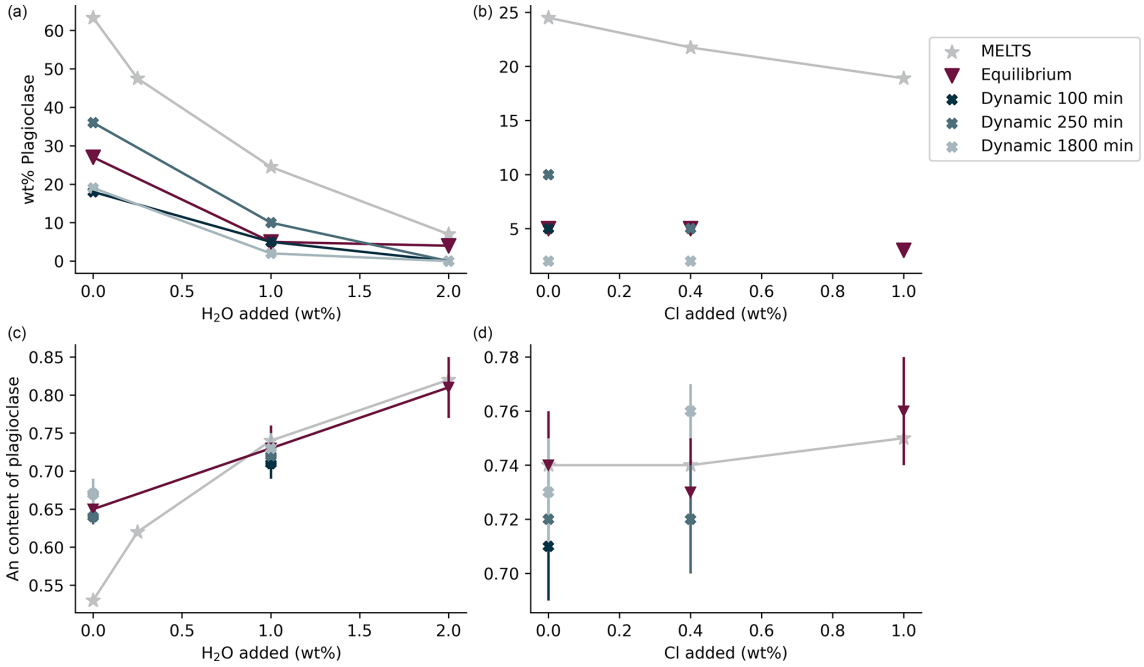

Figure 3. Plagioclase abundance (in wt %) **(a)** and anorthite content of plagioclase **(b)** versus the amount of loaded water (in wt %) in experimental samples. Anorthite contents were calculated based on stoichiometry and charge balance.

Table 5. Results of MELTS modeling (in wt %) with FMQ.

H_2O	0	0.25	1	1	1	2	0	0.25	1	1	1	2	0	0	0.25	0.25	1	1	1
Cl	0	0	0	1	0.4	0	0	0	0	1	0.4	0	0	0	0	0	0	0	0.4
Phase	glass						pl						cpx1	cpx2	cpx1	cpx2	cpx	cpx	cpx1
	5.3	30.9	67.8	80.7	74.0	93.0	63.3	47.5	24.5	18.9	21.75	7	18.7	12.7	8.8	12.8	6	2	3.7
SiO_2	47.5	54.0	53.3	53	52.5	52.0	54.8	52.5	49.6	49.3	49.5	47.5	50.4	48.6	50.3	51.7	50.9	54.2	50.9
TiO_2	4.2	1.3	0.7	0.6	0.6	0.5	–	–	–	–	–	–	0.4	1.3	0.6	0.2	0.4	0.1	0.3
Al_2O_3	12.6	15.7	17.4	17	17.1	18.8	28.7	30.4	32.3	32.5	32.4	33.7	4.1	5.5	5.1	4.0	5.3	3.2	5.4
FeO_{tot}	18.2	10.7	8.1	7.7	7.7	6.5	–	–	–	–	–	–	19.0	12.8	10.3	15.3	8	11.7	7.4
MgO	4.1	4.4	5.9	6.2	6.2	5.9	–	–	–	–	–	–	19.1	14.0	16.2	21.6	17.1	28.9	16.9
CaO	8.3	7.5	8.7	8.9	8.9	10.1	10.9	12.8	15.1	15.3	15.2	16.8	6.8	17.4	17.2	6.9	18	1.9	18.7
Na_2O	3.1	4.6	4.0	3.8	3.8	3.5	5.1	4.2	2.9	2.8	2.9	2.0	0.2	0.4	0.3	0.1	0.2	0.0	0.3
K_2O	1.4	0.9	0.5	0.5	0.5	0.4	0.4	0.1	0.05	0.04	0.04	0.02	–	–	–	–	–	–	–
Cl_2O	–	–	–	1.3	1.3	–	–	–	–	–	–	–	–	–	–	–	–	–	–
P_2O_5	0.5	0.1	0.04	0.04	0.04	0.03	–	–	–	–	–	–	–	–	–	–	–	–	–
H_2O	–	0.8	1.5	1.3	1.3	2.1	–	–	–	–	–	–	–	–	–	–	–	–	–
Mg#	–	–	–	–	–	–	–	–	–	–	–	–	64	66	74	72	79	81	80
An	–	–	–	–	–	–							–	–	–	–	–	–	–
Total	100	100	100	100	100	100	100	100	100	100	100	100	100	100	100	100	100	100	100

FMQ, 1150 °C, 300 MPa; pl signifies plagioclase, and cpx signifies clinopyroxene.

dances in the nominally anhydrous sample are both lower than those calculated by MELTS for 0.25 wt % H_2O (Fig. 3). Consequently, the silicate melt composition of the experimental sample is also different from the calculated one, particularly for Al_2O_3, FeO_{tot}, CaO, MgO, and Na_2O. The FeO_{tot} discrepancy can be associated with the Fe loss in the silicate glass due to Fe incorporation into the Pt or AuPd capsule. For samples with 1 wt % H_2O and 2 wt % H_2O, the discrepancies between experimental and calculated data are generally smaller compared with the nominally anhydrous sample (Fig. 5). These samples experienced less Fe loss than the nominally anhydrous one (18–24 versus 33 wt %, estimated by mass balance calculations).

Therefore, we conclude that the discrepancy between the nominally anhydrous experiment and the MELTS prediction for dry melts can be mainly explained by an increase in wa-

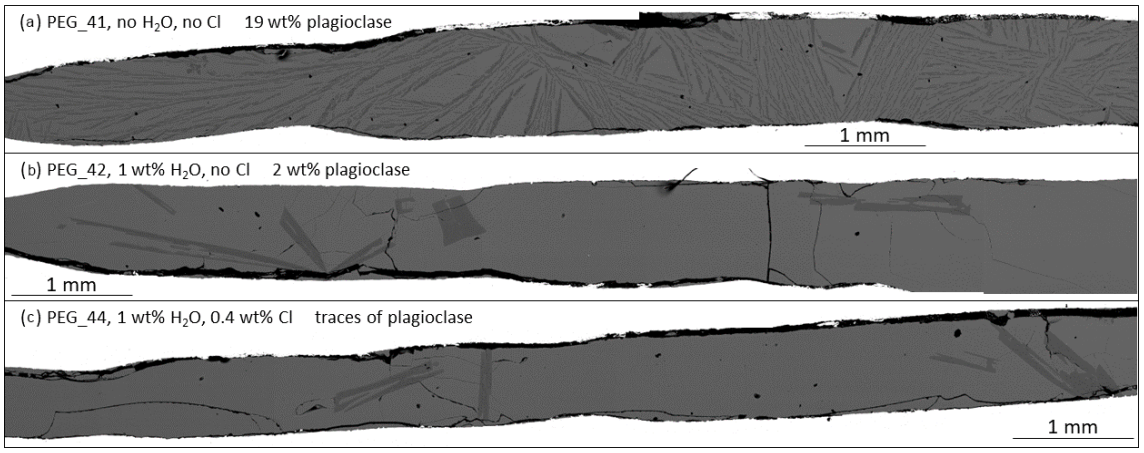

Figure 4. BSE images of approximately half of the capsule of three samples from the dynamic experiment that was held at 1150 °C for 1800 min.

Table 6. Nucleation delay in minutes at 1150 °C.

Mineral	Plagioclase			Clinopyroxene		
	Experiments	Calculations		Experiments	Calculations	
Nucl. type*		Het.	Hom.		Het.	Hom.
0 H_2O, 0 Cl	< 100	3	6	100–250	35	68
1 H_2O, 0 Cl	< 100	27	52	> 1800	n.d.	n.d.
1 H_2O, 0.4 Cl	< 100	41	53	> 1800	n.d.	n.d.
1 H_2O, 1 Cl	100–250	22	41	> 1800	n.d.	n.d.
2 H_2O, 0 Cl	> 1800	260	498	n.d.	n.d.	n.d.

* Nucleation type: heterogeneous or homogeneous. The abbreviation n.d. signifies not determined because it is not present in equilibrium samples.

ter by hydrogen diffusion through the capsule wall during the experiment, which caused redox reactions with the melt (and to a lesser extent by Fe loss). Fe loss to the capsule material leads to a change in the local bulk system composition, which influences the saturation of silicate phases and the respective nucleation delay of those phases. The comparison between MELTS simulations with and without reduced Fe contents only shows minor variations (Table S3). Therefore, we do not expect the Fe loss to significantly impact our results on plagioclase crystallization (the possible effect of Fe loss on clinopyroxene crystallization is discussed in the next paragraph).

4.2 Equilibrium experiment versus dynamic experiments

The dynamic experiments show lower amounts of plagioclase than the equilibrium sample at a given H_2O (and Cl) content (Table 2, Figs. 1–3), suggesting delayed crystallization. Differences in crystallization characteristics of clinopyroxene remain obscured due to a possible effect of Fe loss to the Pt or AuPd capsule, which could potentially limit clinopyroxene crystallization, although MELTS simulations do not predict any significant effect (see previous paragraph). A markedly higher Fe loss in sample PEG_41 (33 wt %; Table 2) than in sample PEG_21 (15 wt %) might explain why clinopyroxene occurs in the latter (Fig. 1g), which lasted 250 min, but not in the former (Fig. 1j), which lasted 1800 min. The absence of clinopyroxene in sample PEG_36 that lasted 100 min, however, suggests the occurrence of delayed nucleation. The composition of the silicate melt in equilibrium and dynamic experiments is indistinguishable within the error bars for most elements (Fig. 5). Only Mg seems to be slightly lower in the equilibrium experiments, probably due to the crystallization of olivine.

Both the experimental data, and the calculations predict an increase in plagioclase nucleation delay with increasing H_2O content and, in particular, a marked increase between 1 wt % H_2O and 2 wt % H_2O. In contrast, experimental data seem to indicate an increase in plagioclase nucleation delay with increasing Cl content, which was not predicted by calculations.

Other notable differences between equilibrium and dynamic samples are the number and size of plagioclase crys-

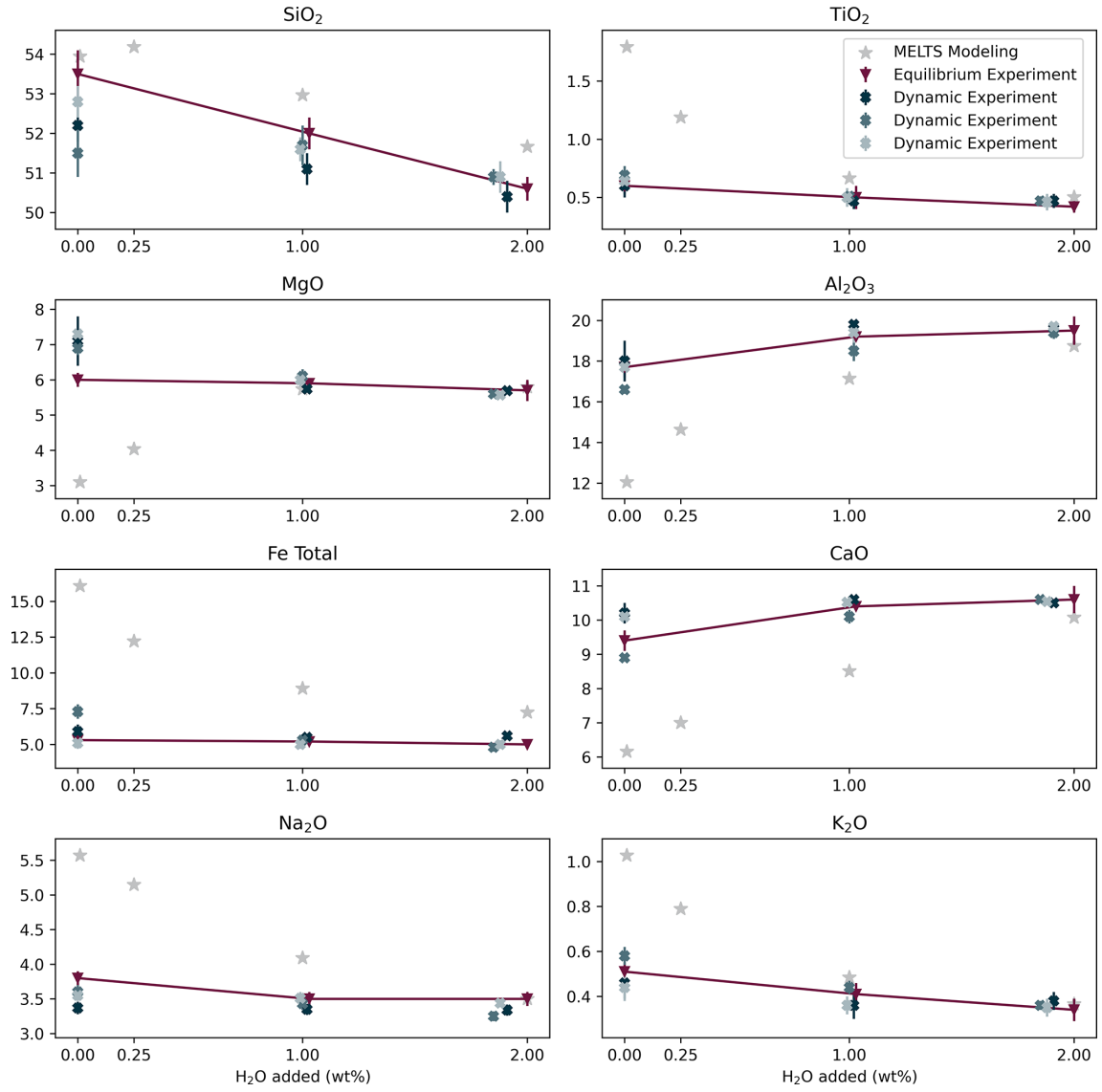

Figure 5. Comparison of melt composition from equilibrium experiments with MELTS.

tals: 5000–30 000 crystals per square millimeter that are a few microns in size (4–7 µm in length) in the equilibrium samples and 100–2000 crystals per square millimeter that are hundreds of microns in size (160–300 µm in length) in the dynamic samples. The lower values in the crystal density correspond to samples containing 1 wt % H_2O, whereas the upper values correspond to nominally anhydrous samples. This suggests that nucleation delay is accompanied by a reduction in the number of crystal nuclei, which favors the developments of larger crystals (Nabelek et al., 2010).

4.3 Effect of water and chlorine on plagioclase abundance and crystal size

In both the equilibrium and dynamic experiments, the effects of H_2O and Cl on plagioclase crystallization are comparable. H_2O reduced plagioclase abundance while increasing plagioclase anorthite content (Fig. 3). The effect of H_2O on plagioclase stability was reported by Sisson and Grove (1993). Chlorine also reduced plagioclase abundance while increasing its anorthite content, albeit to a lesser extent (Fig. 3). The effect of Cl on crystallization of phases from silicate melts is still poorly understood. However, the experiments by Webster and McBirney (2001) revealed that an increased Cl content promotes melting of plagioclase and clinopyroxene plausibly due to an association of Cl with Ca and Mg in aluminosilicate melts.

Moreover, the dynamic experiments revealed the effect of H_2O on plagioclase crystal size, which was not observed in the equilibrium experiment. The longer dynamic experiment (1800 min at 1150 °C) clearly shows that the addition of approximately 1 wt % H_2O reduced the number of plagioclase crystals while increasing their sizes (Fig. 4a, b). In contrast, Cl did not seem to significantly affect the number or size of plagioclase crystals (Fig. 4b, c). These differences in plagioclase size appear to correlate with the calculated nucleation delays, which were significantly increased by water addition and barely affected by chlorine (Table 6).

The effect of H_2O on crystal nucleation was described by Fenn (1977), who observed a decrease in the nucleation density of alkali feldspar with increasing H_2O content in the system $NaAlSi_3O_8$–$KAlSi_3O_8$–H_2O. However, experimental results concerning the influence of H_2O on nucleation kinetics in silicate melts are generally contradictory (Baker and Grove, 1985; Davis et al., 1997; Fenn, 1977; Swanson, 1977), implying that the effect of H_2O cannot be considered independently of other parameters affecting crystallization. Nevertheless, water (i) decreases crystallization temperatures of silicates (Almeev et al., 2012; Sisson and Grove, 1993), (ii) reduces the viscosity of silicate melts (Shaw, 1963), (iii) increases diffusion rates within silicate melts (Watson and Baker, 1991), and (iv) reduces the interfacial free energy between the melt and the growing crystal (Davis et al., 1997; Rusiecka et al., 2020). All of these effects likely favor crystal growth, explaining why the addition of 1 wt % H_2O significantly increases plagioclase size in our dynamic experiments (Fig. 4a, b). Cl, like H_2O, can affect the viscosity of basaltic melts (Webb et al., 2014) and suppress the liquidus temperatures in basalt (Filiberto and Treiman, 2009). Both effects are likely to be less significant than those of H_2O, possibly explaining why the role of Cl on crystal growth seems to be negligible with respect to that of H_2O in our experiments.

4.4 Crystallization kinetics and the degree of undercooling

Crystallization is the thermodynamically driven physicochemical response of a melt to a decrease in temperature relative to the liquidus (saturation) temperature. Crystallization can occur by (1) isobaric cooling (e.g., emplacement of magma), (2) isothermal decompression (e.g., ascending magma), or (3) simultaneous decompression and cooling (Shea and Hammer, 2013). When the melt is rapidly cooled below its liquidus temperature, the term undercooling is used. Undercooling could be due to either heat conduction or an increase in the liquidus temperature itself, for example, due to H_2O loss during magma decompression (Mollard et al., 2012). The degree of undercooling determines the ratio of growth rate to nucleation rate, which determines rock texture. In general, low degrees of undercooling favor crystal growth, whereas high degrees of undercooling favor high nucleation rates (Shea and Hammer, 2013).

Our results indicate that the net effect of H_2O is to reduce the degree of undercooling, allowing plagioclase growth to take precedence over nucleation, resulting in coarse crystallinity. This is consistent with previous experimental findings that H_2O addition reduces the degree of undercooling (Arzilli et al., 2020; Hammer, 2004; Hammer and Rutherford, 2002; Mollard et al., 2012). Moreover, an increase in feldspar size and decrease in abundance with decreasing degree of undercooling has also been reported for (i) basaltic melts in cooling experiments (Vona and Romano, 2013), (ii) hydrous basaltic andesitic magmas in cooling and isothermal decompression experiments (Shea and Hammer, 2013), and (iii) water-saturated rhyolitic melts in decompression experiments (Mollard et al., 2012).

4.5 Implications for the formation of homogeneous mafic pegmatites from the mafic–ultramafic Hamn intrusion, Northern Norway

Despite the lack of a quantitative demonstration, our experiments at 1150 °C and 300 MPa strongly suggest that the addition of 1 wt % H_2O to the Hamn mafic magma reduces the number and increases the size of plagioclase crystals (e.g., Fig. 4a, b). These experimental results support the hypothesis that H_2O is a crucial factor in the formation of coarse grain size in mafic rocks (Beard and Scott, 2018; Larsen and Brooks, 1994; Pentek et al., 2006). In particular, the unzoned pegmatites of the Hamn intrusion exhibit several petrological and geochemical characteristics, suggesting that H_2O and Cl enrichment in the magma may be the cause of the pegmatitic texture (Heckmann et al., 2022): (i) the major and trace element compositions of pegmatites are very similar to those of their host gabbronorites, (ii) the mineral assemblage and mineral chemistry of pegmatites and their host gabbronorites are the same, except for (iii) abundant saussuritization and scapolitization within the pegmatites (not observed in the host gabbronorite). Notably, plagioclase breakdown into zoisite and more sodic plagioclase occurs in the presence of H_2O at high temperatures ($\sim$ 600 °C at 800 MPa and $\sim$ 700 °C at 1 GPa; Goldsmith, 1982). The presence of plagioclase breakdown in unzoned pegmatitic pockets and its absence in host rocks strongly suggest that an aqueous phase existed during the late magmatic stages of pegmatite formation, whereas it was absent or less abundant in host gabbronorites. We propose that the unzoned pegmatitic pockets at Hamn formed from magma that was locally H_2O-richer than the rest of the intrusive body. The presence of Cl-rich phases within the pegmatites (scapolite, chlorapatite, and amphibole) indicates that the magma was Cl-bearing and likely Cl-rich (Heckmann et al., 2022), similar to other mafic pegmatites (Meurer and Boudreau, 1996; Pentek et al., 2006; Sonnenthal, 1992). However, our experiments did not indicate any significant role for Cl in the formation of the pegmatitic texture.

5 Conclusions

Thermodynamic models using the MELTS software are in good agreement with the composition of the residual melt and the endmember composition of plagioclase of the water-bearing equilibrium samples. The discrepancy between the nominally anhydrous phase equilibrium experiment and MELTS prediction for dry melts can be explained by the increase in water caused by hydrogen diffusion through the capsule wall during the experiment, which caused redox reactions with the melt.

The dynamic experiments conducted at 300 MPa under oxygen fugacity conditions ranging from FMQ − 1.65 to FMQ + 0.05 revealed that, in the studied basaltic melt, plagioclase size increased while its abundance decreased with increasing H_2O concentrations. The addition of H_2O reduces undercooling, lowering the nucleation rate versus growth rate ratio, and as a result increases crystal size and decreases plagioclase abundance. In contrast to H_2O, the addition of Cl did not seem to increase the plagioclase size. Cl may not reduce the undercooling as much as water. Consequently, Cl may have a negligible effect on the nucleation and growth rate, which controls the crystal size and abundance.

Plagioclase nucleation was delayed by H_2O. Thermodynamic and kinetic calculations support this experimental finding. H_2O decreases the undercooling while increasing the activation and interfacial free energies compared to bulk free energy per unit volume change. Consequently, the nucleation delay increases. Similarly, Cl increases the nucleation delay of plagioclase in experiments, although the calculations do not support this finding. An increase in the activation and interface free energies reactive to the bulk free energy per change per unit volume could explain this increase.

Data availability. No data sets were used in this article.

Supplement. The supplement related to this article is available online at: https://doi.org/10.5194/ejm-35-1111-2023-supplement.

Author contributions. PH: investigation; writing – original draft; visualization. GM: conceptualization; methodology; investigation; resources; writing – review and editing; project administration; supervision. SSP: funding acquisition; writing – review and editing; project administration; supervision.

Competing interests. The contact author has declared that none of the authors has any competing interests.

Disclaimer. Publisher's note: Copernicus Publications remains neutral with regard to jurisdictional claims made in the text, published maps, institutional affiliations, or any other geographical representation in this paper. While Copernicus Publications makes every effort to include appropriate place names, the final responsibility lies with the authors.

Special issue statement. This article is part of the special issue "Probing the Earth: magma and fluids, a tribute to the career of Michel Pichavant". It is a result of the Magma and Fluids workshop, Orléans, France, 4–6 July 2022.

Acknowledgements. The authors thank Ida Di Carlo, Patricia Benoist-Julliot, Philippe Penhoud, and Sylvain Janiec for their help with the sample preparation and the operation of the analytical instruments. We thank Francois Holtz for the careful handling of the manuscript. Felix Marxer and Chao Zhang are thanked for their detailed and constructive remarks that greatly improved the paper.

Financial support. This research has been supported by the PhD project of the main author (project number 301169). The publication was funded by UiT The Arctic University of Norway. Furthermore, this work was partly supported by the Research Council of Norway through funding to the Norwegian Research School for Dynamics and Evolution of Earth and Planets (DEEP), project number 249040/F60. Further funding was provided by the committee for research training from UiT The Arctic University of Norway, grant number NTF-FU 116-19.

Review statement. This paper was edited by Francois Holtz and reviewed by Chao Zhang and Felix Marxer.

References

Almeev, R. R., Holtz, F., Koepke, J., Parat, F., and Botcharnikov, R. E.: The effect of H_2O on olivine crystallization in MORB: experimental calibration at 200 MPa, Am. Mineral., 92, 670–674, 2007.

Almeev, R. R., Holtz, F., Koepke, J., and Parat, F.: Experimental calibration of the effect of H_2O on plagioclase crystallization in basaltic melt at 200 MPa, Am. Mineral., 97, 1234–1240, 2012.

Arzilli, F., Stabile, P., Fabbrizio, A., Landi, P., Scaillet, B., Paris, E., and Carroll, M. R.: Crystallization kinetics of alkali feldspar in peralkaline rhyolitic melts: Implications for Pantelleria Volcano, Front. Earth Sci., 8, 177, https://doi.org/10.3389/feart.2020.00177, 2020.

Baker, M. B. and Grove, T. L.: Kinetic controls on pyroxene nucleation and metastable liquid lines of descent in a basaltic andesite, Am. Mineral., 70, 279–287, 1985.

Baker, D. R., Rusiecka, M. K., Bilodeau, M., and Kwon, S. Y.: Nucleation delay in the anorthite-diopside binary system: Models and experiments, J. Non-Cryst. Sol., 546, 120255, https://doi.org/10.1016/j.jnoncrysol.2020.120255, 2020.

Bartels, A., Vetere, F., Holtz, F., Behrens, H., and Linnen, R. L.: Viscosity of flux-rich pegmatitic melts, Contrib. Mineral. Petr., 162, 51–60, 2011.

Bartels, A., Behrens, H., Holtz, F., Schmidt, B. C., Fechtelkord, M., Knipping, J., Crede, L., Baasner, A., and Pukallus, N.: The effect of fluorine, boron and phosphorus on the viscosity of pegmatite forming melts, Chem. Geol., 346, 184–198, 2013.

Bartels, A., Behrens, H., Holtz, F., and Schmidt, B. C.: The effect of lithium on the viscosity of pegmatite forming liquids, Chem. Geol., 410, 1–11, 2015.

Beard, J. S.: Characteristic mineralogy of arc-related cumulate gabbros: implications for the tectonic setting of gabbroic plutons and for andesite genesis, Geology, 14, 848–851, 1986.

Beard, J. S. and Scott, S. R.: A model for the high-temperature origin and paradoxical distribution of pegmatites in mafic plutons, Smartville Complex, California, J. Petrol., 59, 3–10, 2018.

Botcharnikov, R., Almeev, R., Koepke, J., and Holtz, F.: Phase relations and liquid lines of descent in hydrous ferrobasalt – implications for the Skaergaard intrusion and Columbia River flood basalts, J. Petrol., 49, 1687–1727, 2008.

Chou, I.-M.: Permeability of precious metals to hydrogen at 2 kb total pressure and elevated temperatures, Am. J. Sci., 286, 638–658, 1986.

Davis, M. J., Ihinger, P. D., and Lasaga, A. C.: Influence of water on nucleation kinetics in silicate melt, J. Non-Cryst. Sol., 219, 62–69, 1997.

Di Carlo, I., Pichavant, M., Rotolo, S. G., and Scaillet, B.: Experimental crystallization of a high-K arc basalt: the golden pumice, Stromboli volcano (Italy), J. Petrol., 47, 1317–1343, 2006.

Fenn, P. M.: The nucleation and growth of alkali feldspars from hydrous melts, Can. Mineral., 15, 135–161, 1977.

Filiberto, J. and Treiman, A. H.: Martian magmas contained abundant chlorine, but little water, Geology, 37, 1087–1090, 2009.

Fokin, V. M., Zanotto, E. D., Yuritsyn, N. S., and Schmelzer, J. W.: Homogeneous crystal nucleation in silicate glasses: A 40 years perspective, J. Non-Cryst. Sol., 352, 2681–2714, 2006.

Fokin, V. M., Zanotto, E. D., and Schmelzer, J. W.: On the thermodynamic driving force for interpretation of nucleation experiments, J. Non-Cryst. Sol., 356, 2185–2191, 2010.

Ghiorso, M. S. and Gualda, G. A.: An H_2O–CO_2 mixed fluid saturation model compatible with rhyolite-MELTS, Contrib. Mineral. Petr., 169, 1–30, 2015.

Ghiorso, M. S. and Sack, R. O.: Chemical mass transfer in magmatic processes IV, A revised and internally consistent thermodynamic model for the interpolation and extrapolation of liquid-solid equilibria in magmatic systems at elevated temperatures and pressures, Contrib. Mineral. Petr., 119, 197–212, 1995.

Goldsmith, J. R.: Plagioclase stability at elevated temperatures and water pressures, Am. Mineral., 67, 653–675, 1982.

Gualda, G. A., Ghiorso, M. S., Lemons, R. V., and Carley, T. L.: Rhyolite-MELTS: a modified calibration of MELTS optimized for silica-rich, fluid-bearing magmatic systems, J. Petrol., 53, 875–890, 2012.

Hammer, J. E.: Crystal nucleation in hydrous rhyolite: Experimental data applied to classical theory, Am. Mineral., 89, 1673–1679, 2004.

Hammer, J. E. and Rutherford, M. J.: An experimental study of the kinetics of decompression-induced crystallization in silicic melt, J. Geophys. Res.-Sol. Ea., 107, B1, https://doi.org/10.1029/2001JB000281, 2002.

Heckmann, P., Palinkaš, S. S., Hansen, H., Iacono-Marziano, G., Rajič, K., Forien, M., and Bergh, S. G.: Petrogenesis of zoned and unzoned mafic pegmatites: An insight from the Palaeoproterozoic mafic-ultramafic Hamn intrusion, Northern Norway, Lithos, 428, 106818, https://doi.org/10.1016/j.lithos.2022.106818, 2022.

Iacono-Marziano, G., Morizet, Y., Le Trong, E., and Gaillard, F.: New experimental data and semi-empirical parameterization of H_2O–CO_2 solubility in mafic melts, Geochim. Cosmochim. Ac., 97, 1–23, 2012.

Jahns, R. H. and Burnham, C. W.: Experimental studies of pegmatite genesis, A model for the derivation and crystallization of granitic pegmatites, Econ. Geol., 64, 843–864, 1969.

Larsen, R. B. and Brooks, C. K.: Origin and evolution of gabbroic pegmatites in the Skaergaard intrusion, East Greenland, J. Petrol., 35, 1651–1679, 1994.

London, D.: Experimental phase equilibria in the system $LiAlSiO_4$–SiO_2–H_2O: a petrogenetic grid for lithiumx-rich pegmatites, Am. Mineral., 69, 995–1004, 1984.

London, D.: Pegmatites, Can. Mineral., 10, 347, ISBN 9780921294474, 2008.

Meurer, W. and Boudreau, A. E.: An evaluation of models of apatite compositional variability using apatite from the Middle Banded series of the Stillwater Complex, Montana, Contrib. Mineral. Petr., 125, 225–236, 1996.

Mollard, E., Martel, C., and Bourdier, J.-L.: Decompression-induced crystallization in hydrated silica-rich melts: empirical models of experimental plagioclase nucleation and growth kinetics, J. Petrol., 53, 1743–1766, 2012.

Mysen, B. and Richet, P.: Silicate melts: properties and structure, ISBN 10: 0444520112, 2005.

Nabelek, P. I., Taylor, L. A., and Lofgren, G. E.: Nucleation and growth of plagioclase and the development of textures in a high-alumina basaltic melt, in: Proceedings of the Ninth Lunar and Planetary Science Conference, Houston, Texas, 13–17 March 1978, 1978.

Nabelek, P. I., Whittington, A. G., and Sirbescu, M.-L. C.: The role of H_2O in rapid emplacement and crystallization of granite pegmatites: resolving the paradox of large crystals in highly undercooled melts, Contrib. Mineral. Petr., 160, 313–325, 2010.

Pentek, A., Molnar, F., and Watkinson, D. H.: Magmatic fluid segregation and overprinting hydrothermal processes in gabbro pegmatites of the Neotethyan ophiolitic Szarvasko Complex (Bukk Mountains, NE Hungary), Geologica Carpathica-Bratislava, 57, 433, 2006.

Pownceby, M. I. and O'Neill, H. S. C.: Thermodynamic data from redox reactions at high temperatures, IV. Calibration of the Re-ReO2 oxygen buffer from EMF and $NiO + Ni$-Pd redox sensor measurements, Contrib. Mineral. Petr., 118, 130–137, 1994.

Robie, R. A. and Bethke, P. M.: Molar volumes and densities of minerals, Unites States Department of the Interior Geol. Surv., 4–21, 1962.

Rusiecka, M. K., Bilodeau, M., and Baker, D. R.: Quantification of nucleation delay in magmatic systems: experimental and theoretical approach, Contrib. Mineral. Petr., 175, 1–16, 2020.

Schindelin, J., Arganda-Carreras, I., Frise, E., Kaynig, V., Longair, M., Pietzsch, T., Preibisch, S., Rueden, C., Saalfeld, S., Schmid, B., and others: Fiji: an open-source platform for biological-image analysis, Nat. Meth., 9, 676–682, 2012.

Shannon, R. D.: Revised effective ionic radii and systematic studies of interatomic distances in halides and chalcogenides, Acta arys-

tallographica Section A: crystal physics, diffraction, theoretical and general crystallography, 32, 751–767, 1976.

Shaw, H. R.: Obsidian-H_2O viscosities at 1000 and 2000 bars in the temperature range 700° to 900 °C, J. Geophys. Res., 68, 6337–6343, 1963.

Shea, T. and Hammer, J. E.: Kinetics of cooling-and decompression-induced crystallization in hydrous mafic-intermediate magmas, J. Volcan. Geotherm. Res., 260, 127–145, 2013.

Sisson, T. and Grove, T.: Experimental investigations of the role of H_2O in calc-alkaline differentiation and subduction zone magmatism, Contrib. Mineral. Petr., 113, 143–166, 1993.

Sonnenthal, E. L.: Geochemistry of dendritic anorthosites and associated pegmatites in the Skaergaard Intrusion, East Greenland: evidence for metasomatism by a chlorine-rich fluid, J. Volcan. Geotherm. Res., 52, 209–230, 1992.

Swanson, S. E.: Relation of nucleation and crystal-growth rate to the development of granitic textures, Am. Mineral., 62, 966–978, 1977.

Taylor, J. R., Wall, V. J., and Pownceby, M. I.: The calibration and application of accurate redox sensors, Am. Mineral., 77, 284–295, 1992.

Thomas, R., Förster, H.-J., and Heinrich, W.: The behaviour of boron in a peraluminous granite-pegmatite system and associated hydrothermal solutions: a melt and fluid-inclusion study, Contrib. Mineral. Petr., 144, 457–472, 2003.

Vona, A. and Romano, C.: The effects of undercooling and deformation rates on the crystallization kinetics of Stromboli and Etna basalts, Contrib. Mineral. Petr., 166, 491–509, 2013.

Watson, E. B. and Baker, D. R.: Chemical diffusion in magmas: an overview of experimental results and geochemical applications, Phys. Chem. Magmas, 120–151, 1991.

Webb, S. L., Murton, B. J., and Wheeler, A. J.: Rheology and the Fe^{3+}–chlorine reaction in basaltic melts, Chem. Geol., 366, 24–31, 2014.

Webster, J. and McBirney, A.: The dramatic effect of chlorine on magmatic phase relations, in: AGU Fall Meeting Abstracts, V32G-06, 2001.

Webster, J. D., Baker, D. R., and Aiuppa, A.: Halogens in mafic and intermediate-silica content magmas, The role of halogens in terrestrial and extraterrestrial geochemical processes: surface, crust, and mantle, 307–430, https://doi.org/10.1007/978-3-319-61667-4_6, 2018.